Journal of Dynamics, Monitoring and Diagnostics, 2025, 4, 264-273
https://doi.org/10.37965/jdmd.2025.828

ISTP
RESEARCH ARTICLE

Design and Experimental Investigations of a Rotary Hybrid Triboelectric-Electromagnetic Energy Harvester for Scavenging Wind Energy

Qi Xiong,[1] Huajiang Ouyang,[1,2] Xiaocui Wang,[3] Jiliang Mo,[1] and Huai Zhao[1]
[1]School of Mechanical Engineering, Southwest Jiaotong University, Chengdu, China
[2]School of Engineering, University of Liverpool, Liverpool L69 3GH, UK
[3]School of Mechanical Engineering, Wenzhou University, Wenzhou, China

(Received 21 May 2025; Revised 15 July 2025; Accepted 11 September 2025; Published online 16 September 2025)

Abstract: With the rapid advancement of the Internet of Things (IoT), the conventional power supply methods encounter challenges such as extensive wiring over long distances and frequent power source replacements. A sustainable power supply is highly desirable for IoT devices. In this study, a novel hybrid triboelectric-electromagnetic harvester is proposed for efficient harvesting of wind energy to sustainably power low-power electronic devices, which integrates a number of sub-triboelectric energy harvesters (sub-TEHs) and sub-electromagnetic energy harvesters (sub-EEHs). The sub-TEH can provide a peak output power of 67 μW when the load resistance is 1 MΩ. The sub-EEH can provide a peak output power of 9.1 mW when the load resistance is 200 Ω. After continuous operation for 15000 cycles, the outputs of both the sub-TEH and the sub-EEH experience no significant attenuation, which indicates good durability of the design. Under a wind speed of 11 m/s, over 100 LEDs can be lit up. And a temperature–humidity sensor is able to work continuously when powered by the hybrid energy harvester via a rectifier circuit. The hybrid energy harvester exhibits good output performance and long-term stability with a simple structure and low production cost, which has great potential in wind energy harvesting and wireless environmental monitoring applications.

Keywords: electromagnetic; hybrid energy harvester; triboelectric; wind energy

I. INTRODUCTION

In recent years, the rapid development and increasing demand for the Internet of Things (IoT), wearable electronics, wireless sensor networks (WSN) and micro-electro-mechanical systems (MEMS) have created an urgent need for novel and efficient energy supply [1–3]. Traditional batteries for low-power electronic products have limitations, such as limited life, frequent replacement or recharging, and environmental concerns. Due to the development of integrated circuits, the power consumption of many devices has been reduced to below a few μW [4]. Therefore, small-scale energy harvesting for low-power electronic devices has attracted great attention from researchers in various fields [5,6].

Various forms of clean energy exist in the environment, such as wind energy [7], solar energy [8], mechanical vibration energy [9], wave energy [10], and human movement energy [11]. These clean energy sources can be converted into electricity through various methods, including electromagnetic induction [12,13], electrostatic [14–16], piezoelectric transduction [17,18], and triboelectrification [19–21]. Since the triboelectric nanogenerator (TENG) was first proposed by Prof. Zhonglin Wang's group in 2012 [22], triboelectric energy harvesting has attracted more and more attention in recent years. It has shown advantages of high output voltage, high energy conversion efficiency, low cost, and abundant choices of materials, demonstrating the great potential of harvesting mechanical energy using organic [23,24] and inorganic materials [25].

A triboelectric energy harvester (TEH) operates based on the combination of triboelectrification effect and electrostatic induction, which take place between two thin organic/inorganic films that exhibit distinct surface electron affinities. When a mechanical force induces relative motion (tangential slip or normal separation) between the surfaces, an electric potential difference is generated, driving electron flow between the electrodes [26]. Generally, TEHs work in four working modes, namely vertical contact-separation mode, lateral sliding mode, single-electrode mode, and free-standing triboelectric layer mode [27]. Here is a brief review of some designs with different working modes. In nature, the direction and frequency of most mechanical vibrations are random. Yang [28] *et al.* proposed a three-dimensional TENG, which can operate in both vertical contact-separation mode and horizontal sliding mode to harvest mechanical vibration energy. Researchers also used S-shaped compliant beam [29], clamped beams [30], and cantilever beams [31] in TENGs to enhance vibration energy harvesting efficiency. Zhao *et al.* [7] proposed a new independently programmed TENG banner, which can generate current from the wind in any directions for efficient wind energy harvesting. Chen *et al.* [32] also studied a rotating disk wind energy TENG for self-driven air purification and electrochemical oxidation SO_2. To address power supply challenges in marine environmental monitoring, a highly symmetric 3D spherical-shaped water-based triboelectric nanogenerator (SWTENG) was developed [33], used to scavenge low-frequency water wave energy. In addition, some researchers have combined TENGs with

Corresponding author: Huai Zhao (e-mail: zhaohuai@swjtu.edu.cn)

chaotic pendulum structures [34] and proposed a spherical hybrid triboelectric nanogenerator (SH-TENG) [35] for enhancing wave energy harvesting. Some researchers have applied TENGs to self-powered sensing, providing a promising solution to power supply of IoT sensors [36,37].

At present, energy harvesters based on a single energy transduction mechanism usually cannot provide sufficient power supply for electronic devices. It is well known that TEHs have high output voltage and low output current [36]. An effective way to improve the output current is to integrate a number of sub-TEHs in a single design and synchronize their outputs. Another approach is to integrate TEHs with other types of energy harvesters, such as electromagnetic energy harvester (EEHs), to form a hybrid harvester. The EEHs usually have high output current and low output voltage [36], and as a traditional power generation method, EEHs exhibit good stability. Therefore, a hybridization of TEHs and EEHs can take advantage of their complementary features. Due to the high efficiency of the TEHs at low frequency and the high efficiency of the EEHs at high frequency, their combination can expand the working bandwidth of the harvester [37], making it more suitable for specific applications. Hybrid triboelectric-electromagnetic energy harvesters have made significant progress in harvesting various forms of low-frequency mechanical energy. However, there are still some challenges in terms of structural rationality and ease of use.

In this work, inspired by engine pistons, we proposed a novel hybrid energy harvester for wind energy, which includes a number of cylindrical magnets behaving like engine pistons. The magnets move upward and downward periodically under the excitation of a rotating wind cup, enabling the hybridization between electromagnetic energy harvesting and triboelectric energy harvesting. A number of EEHs and TEHs are integrated in a single device, which efficiently improve the harvesting efficiency for wind energy. The main structure of the harvester is manufactured from resin materials through 3D printing technology. The device is compact and cost-effective, which consists of four sub-TEHs and four sub-EEHs. The working mechanism of the hybrid energy harvester is based on the contact-separation between the PTFE films and the copper films, along with the magnetic flux changes in the coils caused by the moving magnets, enabling both the sub-TEHs and the coils (sub-EEHs) to generate electricity. The output performance of sub-TEHs and sub-EEHs is studied on a center for tribology research friction and wear testing machine (CETR) and in a wind tunnel. This work aims to present an efficient harvester for scavenging wind energy and providing a sustainable power supply for wireless environmental monitoring applications.

The outline for the rest of this paper is as follows: Section II describes the architecture of the proposed harvester, the basic working mechanism, and the finite element simulation analysis. Section III presents the experimental system setup and the measurement of the electrical outputs. In Section IV, a wind tunnel test rig is constructed to investigate the capability of the harvester for extracting wind energy, and the potential applications of the harvester are explored. Finally, the main conclusions are summarized in Section V.

II. DESIGN, WORKING MECHANISM, AND SIMULATION

A. PROTOTYPE DESIGN

This study presents a novel hybrid triboelectric-electromagnetic energy harvester, which includes four sub-TEHs and four sub-EEHs, as shown in Fig. 1. The main structure of the energy harvester is composed of a fixed disk, a rotating disk, a wind cup, and a shell, which are 3D-printed using a white resin material. The rotating disk is connected to the wind cup via an axle, which is able to rotate around its center. There are four grooves spaced 90° apart on the rotating disk, in which four NdFeB permanent magnets (diameter of 40 mm and height of 5 mm) with alternating distribution of N and S poles are embedded, respectively.

The fixed disk has a diameter of 160 mm and a thickness of 6 mm. There are four hollow cylinders (inner diameter: 41 mm, external diameter: 44 mm, height: 40 mm) located on the fixed disk. Small windows are cut on the cylinders to facilitate the connection between electrodes of sub-TEHs and wires. Four bottom plates are fixed on the bottom of the hollow cylinders, which are covered by a copper film and a PTFE film. Four movable

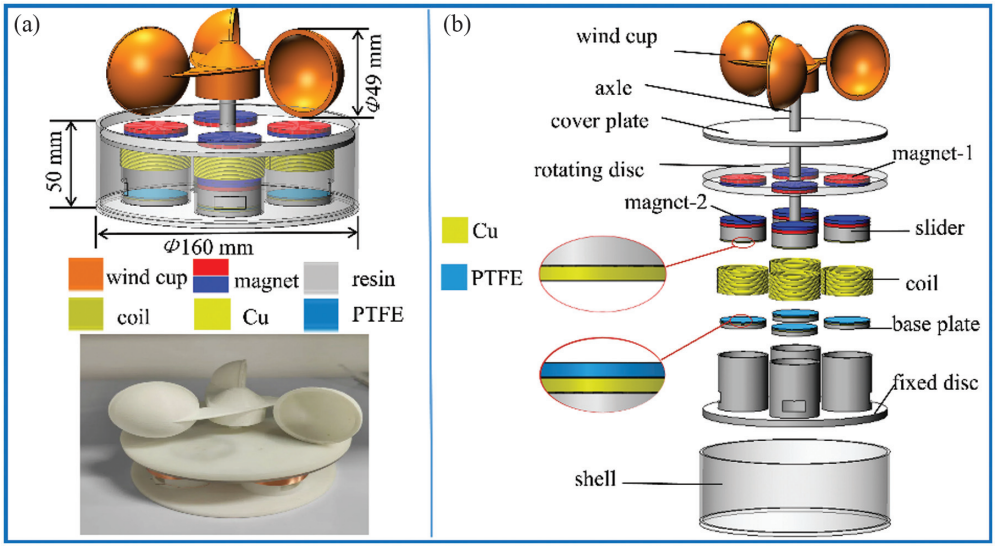

Fig. 1. Structural design of the hybrid energy harvester: (a) overall configuration and (b) exploded view.

sliders are inside the hollow cylinders. Magnets are fixed on the top of the sliders. And the bottom surfaces of the sliders are covered by copper films. Four coils with 540 turns are fixed on the external surface of the hollow cylinders, made of wires with a diameter of 0.3 mm. These films on the sliders and the bottom plates form the four sub-TEHs working in contact-separation mode. And the magnets and coils form four sub-EEHs.

B. WORKING MECHANISM

Figure 2 shows the working mechanism of the triboelectric-electromagnetic energy harvester. As depicted in Fig. 2(a), at the initial stage, the S poles of the bottom magnets are aligned with the N poles of the top magnets. Due to the magnetic attraction between opposite poles, the bottom magnets move upward, which drive the sliders to slide upward. When the rotating disk turns 90 degrees, driven by the wind cup, the S poles of the bottom magnets aligns with the S poles of the top magnets, creating repulsive forces that drive the sliders to move downward. As the disk continues to rotate, the sliders induce periodic vertical motion, thereby activating the sub-TEHs and sub-EEHs.

The charge transfer process for the sub-EEH is illustrated in Fig. 2(b). From Faraday's law of electromagnetic induction, it can be known that when a magnet travels from its initial position away from a copper coil, the magnetic flux through the coil changes, which induces an electromotive force, leading to a current in the closed loop. When the magnet returns to its initial position, the closed loop generates an equal current in the opposite direction. Therefore, the repetitive up-and-down motion of the magnet can generate an alternating current.

The charge transfer process for the contact-separation TEH is illustrated in Fig. 2(c). In the initial state, no induced charges are generated and there is no potential difference between the two electrodes. When the metal film comes into contact with the dielectric film driven by the slider, the triboelectric effect causes the dielectric film to generate a net negative charge and the metal film to generate a net positive charge (Fig. 2(c)-I). The separation between the metal film and the dielectric film creates a potential difference between the two electrodes due to the opposite triboelectric charges, under open-circuit conditions. When a load is connected to the two electrodes, electrons are driven to flow through the load between the electrodes (Fig. 2(c)-II). As the metal film and the dielectric film separate further, the potential difference continues to increase, and the current continues to flow through the load until an electrical equilibrium is established (Fig. 2(c)-III). When the slider moves backward and the electrodes approach each other, an opposite current is generated through the external load (Fig. 2(c)-IV). Therefore, during the continuous rotation of the disk, alternating current is generated through the external load circuit.

As shown in Fig. 2(d), the sub-TEHs can be equivalently modeled by an equivalent capacitance C and an ideal voltage source V_{oc} [38]. The electricity generation equation for a sub-TEH can be written as:

$$R\frac{dQ}{dt} = V(t) = -\frac{1}{C}Q + V_{oc} \tag{1}$$

where R is the external resistance of the circuit and Q is the charge transfer between the two electrodes. The open-circuit voltage and equivalent capacitance for the sub-TEHs can be expressed as follows:

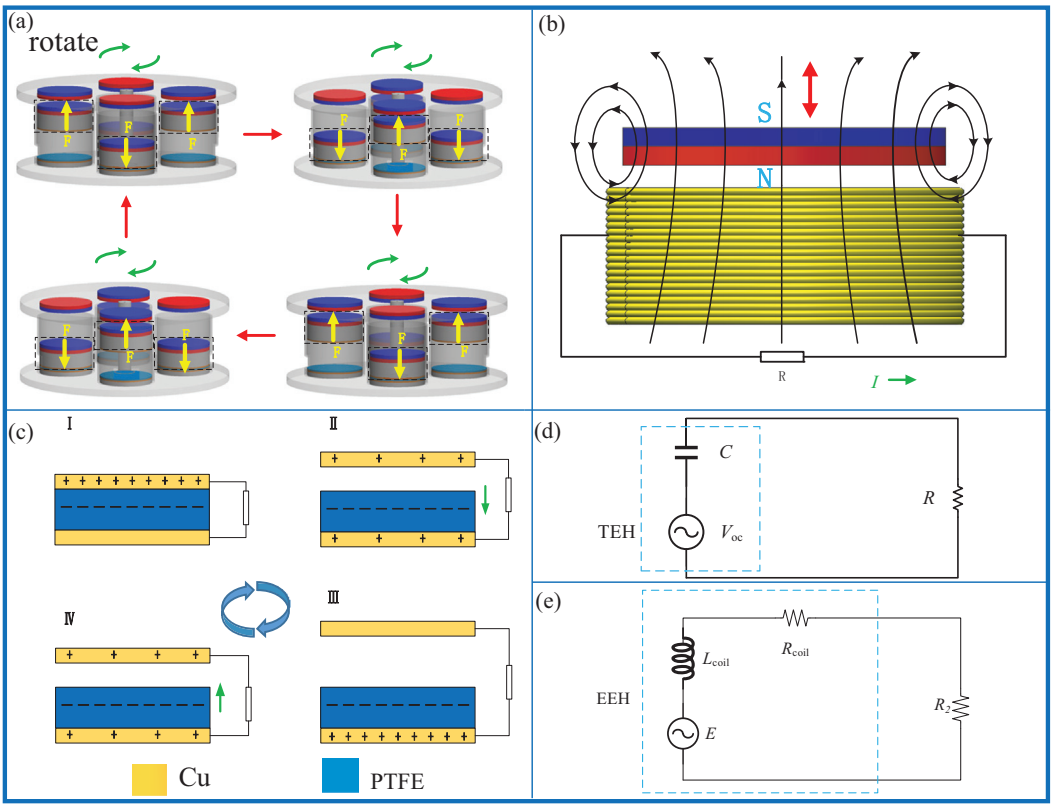

Fig. 2. Working mechanism of the hybrid harvester: (a) working diagram, (b) the charge generation process in the sub-EEHs, (c) the charge generation process in the sub-TEHs, (d) equivalent circuit of TEHs, and (e) equivalent circuit of EEHs.

$$V_{oc} = \frac{\sigma x(t)}{\varepsilon_0} \tag{2}$$

$$C = \frac{\varepsilon_0 S}{d_0 + x(t)}$$

where S is the area of the dielectric layer, and the ratio of the dielectric material thickness to its dielectric constant is defined as the effective thickness d_0. ε_0 is the vacuum permittivity, σ is the surface charge density, and $x(t)$ is the distance between the two dielectric layers.

The equivalent circuit of a sub-EEH is shown in Fig. 2(e), which can be mathematically represented by [39]:

$$L_{coil} \cdot \dot{I} + (R_{coil} + R_2)I = E = \gamma \dot{Z} \tag{4}$$

where R_{coil} is the equivalent resistance of the coil, L_{coil} is the equivalent inductance of the coil, R_2 is the external resistance, and E is the induced voltage of the coil. I denotes the current in the circuit. Z is the relative displacement between the magnetic and the coil. γ is electromagnetic coupling coefficient.

C. MULTIPHYSICS PERFORMANCE SIMULATION

Figure 3(a) illustrates the distributions of the electric potential difference at different separation distances. According to the simulation results, the potential difference is zero when the two triboelectric layers are in contact. The potential difference increases with the separation distance between the triboelectric layers. When the layers reach their maximum separation, the potential difference reach its maximum value. As shown in Fig. 3(b), the motion of the top triboelectric layer is a sine function, resulting in a sinusoidal potential difference between the two electrodes, which are consistent with the theoretical foundation of the triboelectric energy harvesting presented in Eq. (2).

Figure 3(c) shows that the magnet moves periodically up and down within the coil, causing changes in the magnetic flux and inducing voltage. Figure 3(d) illustrates the relationship between the induced voltage and the magnet velocity, which indicates that the voltage of the coil increases linearly with the velocity of the magnet. From Eq. (4), it is known that the induced voltage across the coil is $\gamma \dot{Z}$, which keeps a linear relationship with the velocity of the bottom magnet.

III. FUNDAMENTAL PERFORMANCE CHARACTERIZATION

A. EXPERIMENT SETUP

The experimental system for the performance test of the hybrid energy harvesting is shown in Fig. 4. The rotating motor of the CETR is used to drive the harvester, with its angular speed adjustable from 0.001 to 7000 rpm. The VICTOR-240S multifunctional oscilloscope is used to measure the output voltage of the device. All the data are transmitted to the computer for storage and analysis.

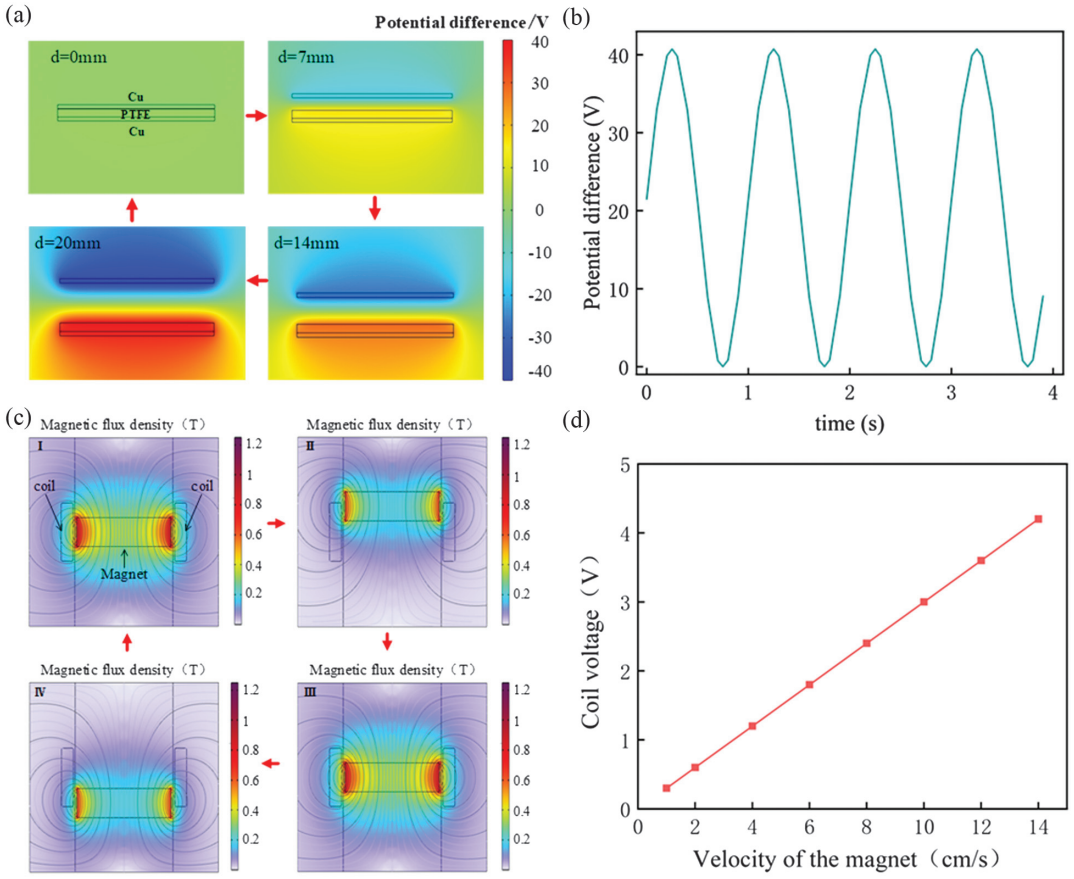

Fig. 3. Simulation of a sub-TEH and a sub-EEH: (a) potential distribution of a sub-TEH at different spacing distances, (b) a sub-TEH surface potential curve, (c) a sub-EEH flux density distribution at different positions, and (d) a sub-EEH voltage curve with velocity of the magnet.

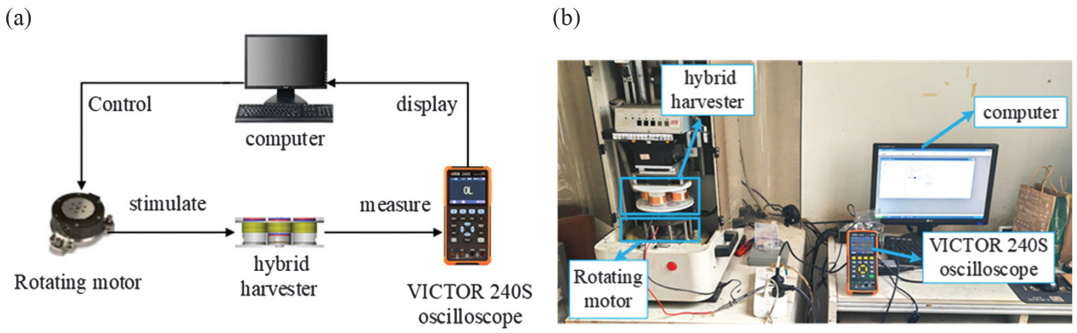

Fig. 4. Experiment system for the performance test of the hybrid harvester.

B. RESULTS AND ANALYSIS

For measuring the output voltage of the sub-TEH at different speeds, a load resistor is wired to the electrodes of a sub-TEH, as shown in Fig. 5(a). The corresponding power output of the sub-TEH is measured at different rotational speeds, namely 60 r/min, 120 r/min, 180 r/min, 240 r/min, 300 r/min, 360 r/min, 420 r/min, and 480 r/min. Figure 5(b) shows the output voltage of the sub-TEH versus the rotation speed. Specifically, as the speed increases from 60 r/min to 300 r/min, the output voltage increases from 3.1 V to 13 V.

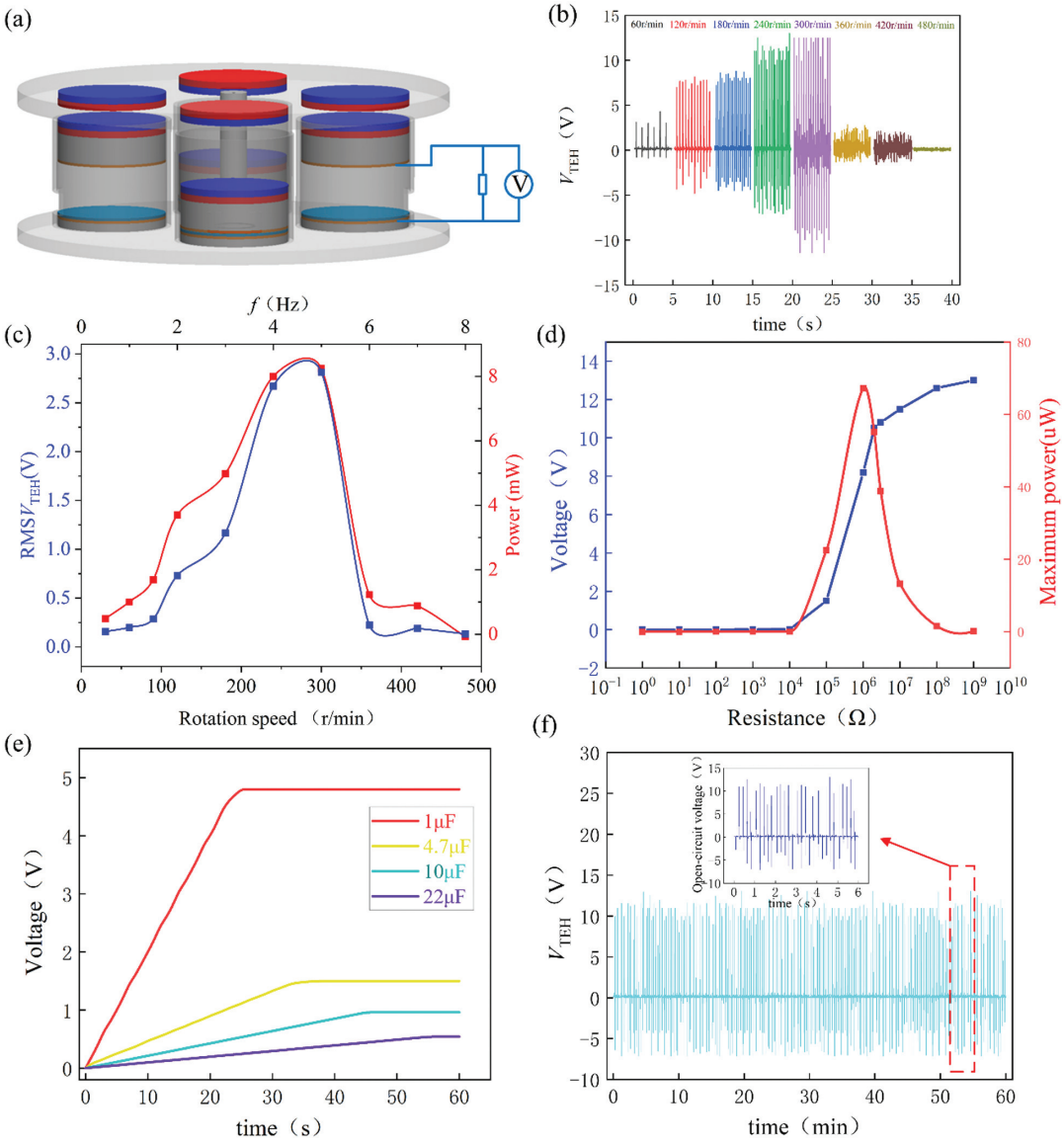

Fig. 5. Experiments of a sub-TEH: (a) measurement circuit, (b) measured voltage under different rotational speeds, (c) the RMS voltage and power at different speeds, (d) peak power and voltage under different load resistances, (e) DC voltage with different capacitors, and (f) voltage after 15000 cycles.

However, beyond 360 r/min, the output voltage begins to decrease, eventually reaching 0.12 V at 480 r/min. This phenomenon is closely related to the operational principles of the hybrid harvester and the mechanism of the sub-TEHs. In the range from 60 r/min to 300 r/min, as the motor speed increases, the frequency of magnetic interactions within the device also increases due to repulsive and attractive forces, accelerating the movement of the magnet. According to magnetic force principles, the closer the magnets are, the higher the magnetic force, which increases the kinetic energy imparted to the slider. This enhances the contact between the friction layers of the sub-TEH, leading to the higher surface charge density. However, when the speed exceeds 360 r/min, the magnet moves too quickly, causing the slider to move upward by repulsive forces before it can fully impact with the friction layer, resulting in insufficient contact between the friction layers compared with lower speeds, thereby reducing the output voltage. The signals of output voltage show obvious fluctuation, which results from the nonsmooth movement of the sliders. During operation, the sliders could be stuck occasionally, which can be improved by reducing the surface roughness of the internal surfaces of the hollowed cylinders on the fixed disk.

Figure 5(c) illustrates the root-mean-square (RMS) output voltage of the sub-TEH under different rotation speeds. The corresponding frequencies of the motion of the slider is calculated based on the rotation speeds. As the speed increases from 60 r/min to 300 r/min, the frequency of the slider increases from 1 Hz to 5 Hz, and the RMS voltage rises from 0.288 V to 2.85 V. Further increasing the speed from 300 r/min (5 Hz) to 480 r/min (8 Hz) leads to the decrease of RMS voltage from 2.85 V to 0.1 V. The peak power for different load resistances is measured at 180 r/min, as shown in Fig. 5(d). The experimental results show that the optimal resistance of the sub-TEH is approximately 1 MΩ, and the corresponding power is 67 μW. Based on the contact area of 3.14 cm^2, the areal power density is calculated to be 85.4 $\mu W/cm^2$. In order to test the charging performance of the sub-TEHs, a sub-TEH is connected to a rectifier. Then the rectified voltage is fed into a capacitor. A handheld digital oscilloscope (VICTOR 240S) with a high impedance probe is used to measure the DC voltage across the capacitor. Figure 5(e) illustrates the voltages across different capacitors (1 μF, 4.7 μF, 10 μF, and 22 μF) at 180 r/min. It can be seen that the charging speed decreases with the increase in the capacitance. A DC voltage of 4.8 V can be obtained with a capacitor of 0.22 μF, which decreases to 0.54 V when a capacitor of 22 μF is utilized. Figure 5(f) illustrates the voltage of the sub-TEH during continuous operation for 15000 cycles. The output voltage does not decrease obviously after 15000 cycles, which indicates good durability of the sub-TEHs.

According to impedance matching theory, the optimal load resistance for EEHs should be approximately equal to the coil resistance [40]. The electric resistance of a coil is measured as 200 Ω. Therefore, a resistor of 200 Ω is used as the load resistor for each sub-EEHs in the experiment. The measured output voltage of the single sub-EEH under different rotational speeds and frequencies is shown in Fig. 6(a). The peak voltage increases from 2.24 V at

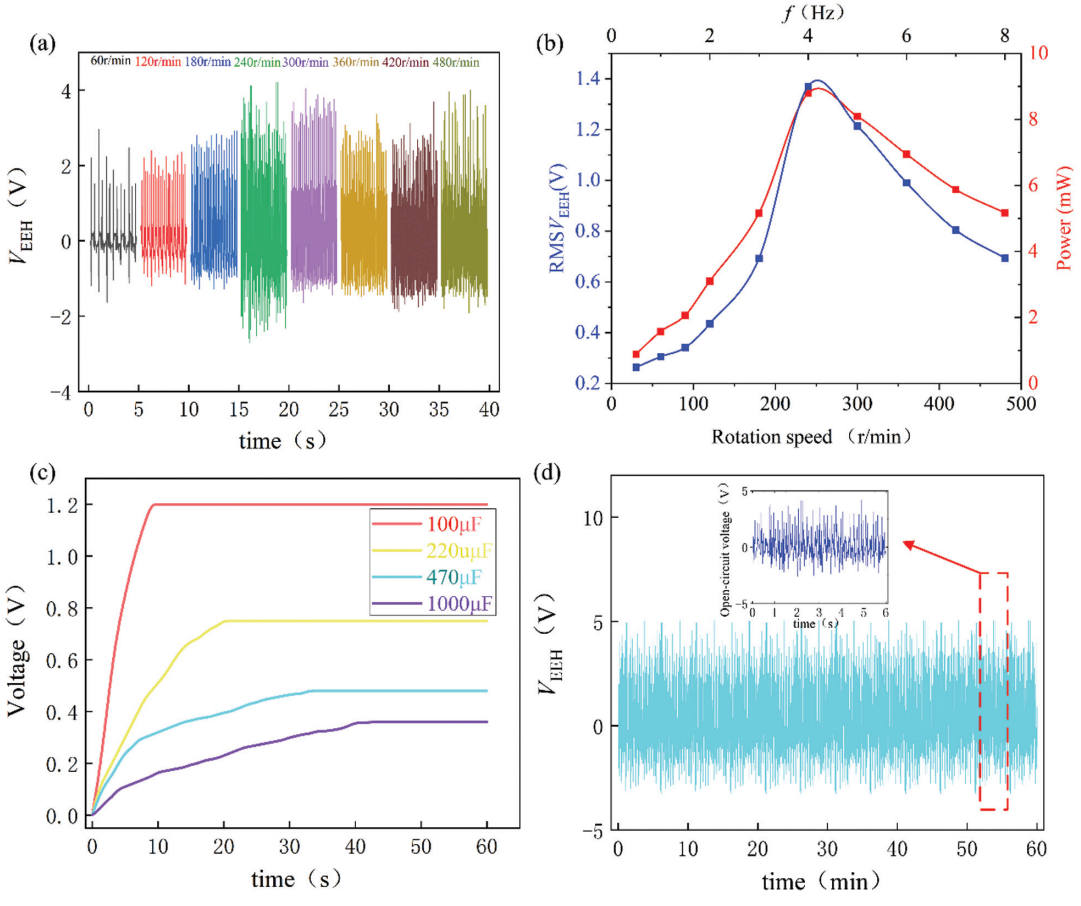

Fig. 6. Experiments of a sub-EEH: (a) measured voltage and power under different rotational speeds, (b) the RMS voltage and power at different speeds, (c) DC voltage with different capacitors, and (d) voltage after 15000 cycles.

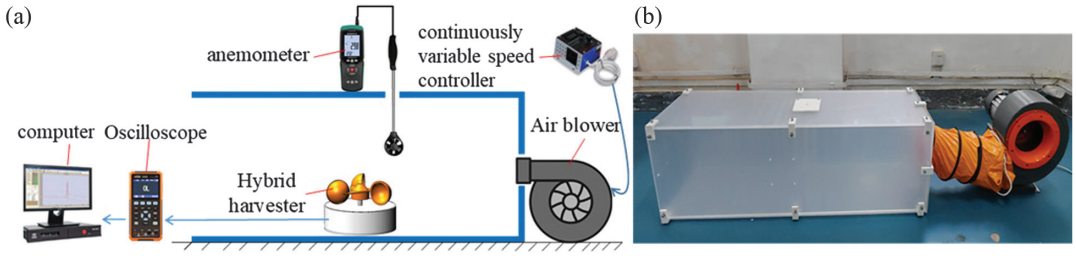

Fig. 7. Schematic of the wind tunnel test rig.

60 r/min (1 Hz) to 4.12 V at 240 r/min (4 Hz). However, the peak voltage decreases from 4.12 V at 240 r/min (4 Hz) to 3.2 V at 480 r/min (8 Hz). The maximum power of the sub-EEH is calculated to be 9.7 mW and the corresponding volumetric power density is 0.04 mW/cm^3. Unlike the sub-TEH, the sub-EEH does not exhibit a sharp drop in output voltage, which is due to its working principle. The output voltage of the sub-EEH is primarily influenced by the relative motion speed between the magnet and coil [44]. When the rotational speed rises from 60 r/min to 240 r/min, the velocity of magnet also increases. However, when the speed exceeds 240 r/min, the magnet inside the hollow cylinder does not have enough time to complete its full downward movement before being attracted by the next magnet in the rotating disk. This phenomenon results in a slight decrease in the velocity of magnet and output voltage. Figure 6(b) illustrates the RMS output voltage of the sub-EEH under different rotational speeds. As the speed increases from 60 r/min to 240 r/min, the RMS voltage rises from 0.315 V to 1.343 V. However, as the speed increases from 240 r/min to 480 r/min, the RMS voltage drops from 1.343 V to 0.872 V.

Due to the output current of the sub-EEH is larger than that of the sub-TEH, capacitors with higher capacitance values (100 μF, 220 μF, 470 μF, and 1000 μF) are used to characterize the charging performance in this experiment. In the following experiments, a constant speed of 180 r/min is set. The DC voltage with different capacitors (100 μF, 220 μF, 470 μF, and 1000 μF) is shown in Fig. 6(c). It can be seen that the charging speed decreases with the increase in the capacitance. A DC voltage of 1.2 V can be obtained with a capacitor of 100 μF, which decreases to 0.36 V when a capacitor of 1000 μF is utilized. Figure 6(d) illustrates the voltage of the sub-EEH after 15000 cycles. As seen from the figure, the output voltage nearly experiences no attenuation, and the maximum voltage of the sub-EEH can still reach 4.12 V in this environment, further confirming the good durability of the sub-EEHs.

IV. POTENTIAL APPLICATIONS

The proposed energy harvester is capable of harvesting wind energy from the natural environment. In order to test the capability of the harvester for harvesting wind energy, a wind tunnel test rig is constructed, as shown in Fig. 7. The main structure of the wind tunnel is constructed using transparent acrylic panels in which the proposed harvester is fixed. The air blower is utilized to generate wind flows in the tunnel with certain velocities, which could be measured by an anemometer. A continuously variable speed controller is added to adjust the wind speed, and an oscilloscope is used to measure the performance of the hybrid harvester under different wind speeds.

Figure 8(a) and (b) illustrate the voltage levels of the sub-TEH and the sub-EEH at a wind speed of 11 m/s, with peak voltages reaching 7.65 V and 2.1 V, respectively. It can be seen that the voltage of the sub-EEH has sharp peaks, which result from the motion of the slider. As mentioned in Section C, the output voltage of the coil has a linear relationship with the velocity of the sliders. During the rotation of the wind cup, the rotating magnets produce attractive and repulsive forces alternatingly on the sliders. When attracted, a slider moves upward and its velocity increases sharply due to the strong magnetic attractive force until impact takes place at the top. While under the repulsive force, a slider moves downward with large accelerations, finally impacting the bottom surface. The velocity of the slider increases or decreases sharply in operation, resulting in sharp peaks in the voltage signal of the sub-EEH. As shown in Fig. 8(c) and Fig. 8(d), the peak output voltages of the sub-TEH and the sub-EEH vary with different wind speeds. The peak voltage of the sub-TEH increases from 2.5 V at 5 m/s to 11.23 V at 15 m/s, while the peak voltage of the sub-EEH increases from 0.84 V at 5 m/s to 2.7 V at 15 m/s.

The capacitor charging performance of the energy harvester is evaluated using a 100 μF capacitor at a wind speed of 11 m/s. It is evident that when the sub-TEHs and the sub-EEHs are connected in parallel, the charging rate is significantly greater compared with individual sub-TEH and sub-EEH configurations, resulting in higher voltage levels, as depicted in Fig. 9(a). With the rapid advancement of electronic technology, an increasing number of low-power electronic devices are emerging. In practical applications, energy harvesters can power LED arrays, serving as a fundamental method of experimental validation. Figure 9(b) demonstrates the ability of powering 100 LEDs under wind blowing. Unlike LEDs, which can be driven by AC voltage or pulse power, the hygrograph shown in Fig. 9(c) and (d) requires a DC power source. Consequently, in this experiment, a 1000 μF electrolytic capacitor was used as an energy storage unit to power the hygrograph. The energy harvester's ability to sustain continuous operation of the hygrograph under wind excitation exhibits its potential for harvesting wind energy in natural environments, making it suitable for wireless sensor power supplies.

V. DISCUSSIONS

According to the experimental results above, the maximum output power of the sub-TEHs is 67 μW, while that of the sub-EEHs reaches 9.1 mW. A comparison between the

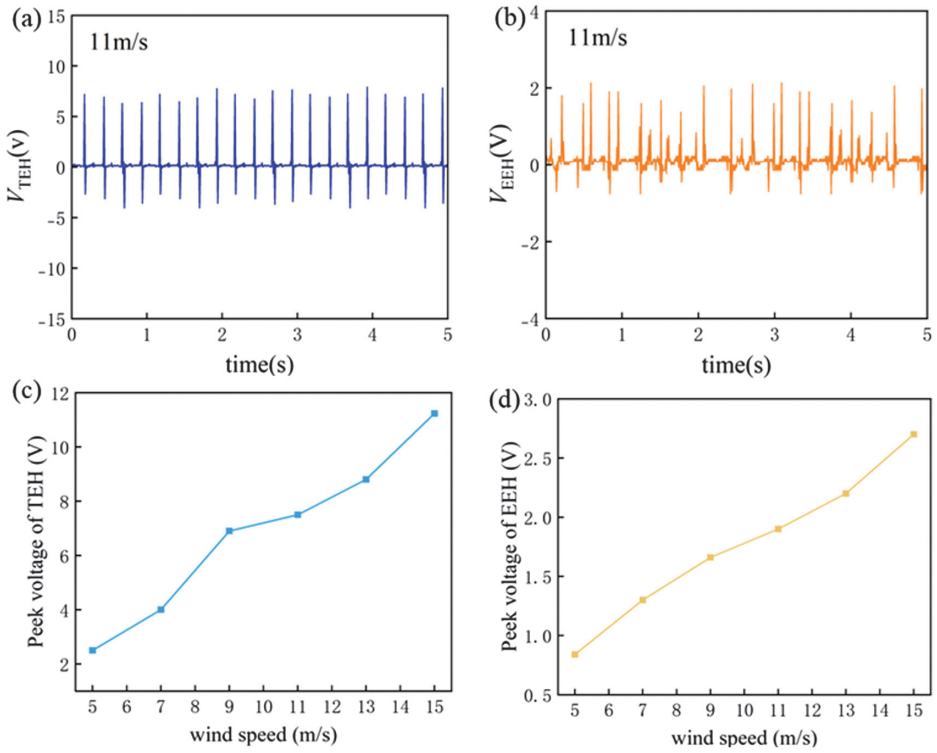

Fig. 8. (a) and (b) Output voltages of a sub-TEH and a sub-EEH at 11m/s. (c) and (d) Peak voltage of a sub-TEH and a sub-EEH at different wind speeds.

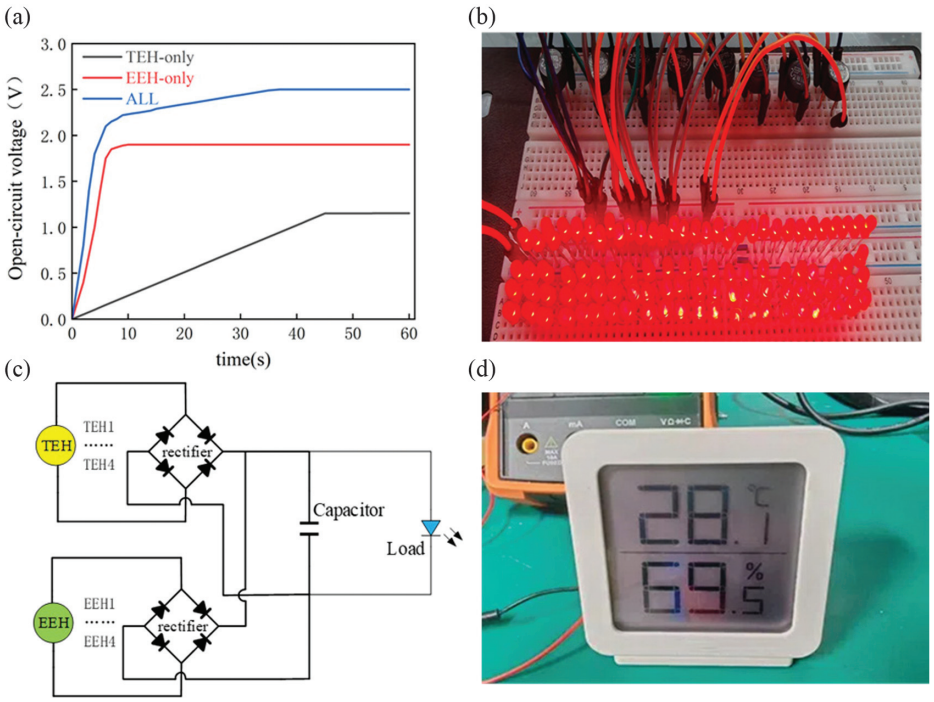

Fig. 9. (a) DC voltage with a capacitor of 1000 μF. (b) LEDs powered by the hybrid harvester. (c) Circuit for powering the hygrothermograph. (d) The hygrothermograph powered by the harvester.

proposed design and a number of reported hybrid energy harvesters is shown in Fig. 10. As observed, the output power of the sub-TEHs ranks the second, while the power of the sub-EEHs ranks the first among the several hybrid energy harvesters. Although the proposed energy harvester is not the most efficient one, it exhibits outstanding performance compared with most of the reported harvesters. It is worth noting that common commercial films with a low surface charge density are used in this design, resulting in a low output power of the sub-TEHs, which can be

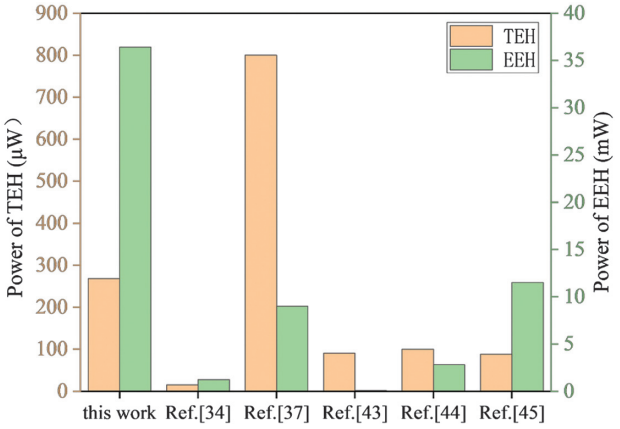

Fig. 10. Comparison between the proposed energy harvester and some reported hybrid triboelectric-electromagnetic energy harvester.

greatly improved by functionalized materials or surface modification.

The purpose of hybridization of TEHs and EEHs is to take advantage of their complementary features. Specifically, TEHs have a high output voltage and EEHs have a high output current. When combined, they more likely meet the requirement of particular applications. Furthermore, the hybridization of TEHs and EEHs can be used to broaden the operating bandwidth of the harvester due to the high efficiency of TEHs at low frequencies and high performance of EEHs at high frequencies [38].

However, the practical application of the proposed design still faces several challenges. For instance, due to friction between various components of our harvester, it cannot operate normally at wind speeds below 3 m/s. Moreover, the sub-TEHs have large internal resistance. Based on the theory of impedance matching, the optimal output power is achieved when the load resistance is approximately equal to the internal resistance of the harvester. But in actual operation, it is unlikely for the load to reach a high-level resistance. In addition, as the device contains different types of power generation units, an efficient power management approach is required to manage the outputs and minimized power loss. For most energy harvesters, cost of production is also a challenge, which would be improved as hardware materials and manufacturing technologies become cheaper.

VI. CONCLUSIONS

In summary, a hybrid triboelectric-electromagnetic energy harvester for wind energy is proposed in this work, which consists of four sub-EEHs and four sub-TEHs in contact-separation mode. The device is cost-effective and can simultaneously drive two types of power generation units in wind flows. The performance of the hybrid energy harvester is investigated through both multiphysics simulations and experiments. The maximum output power of the sub-TEH is 67 μW, while that of the sub-EEH is 9.1 mW. When placed in a wind tunnel, the hybrid energy harvester can power over 100 LED lights. Through a rectifier circuit, the proposed design is able to power a hygrometer to operate continuously. This work presents a novel hybrid triboelectric-electromagnetic energy harvester with good performance, which provides a potential solution for wind energy harvesting.

ACKNOWLEDGMENTS

This research receives financial support from National Natural Sciences Foundation of China (Grant No. 12272324 and Grant No. 12432002), Central University Science and Technology Innovation Project (Grant No. 2682024CX096), and Sichuan Provincial Natural Science Foundation Youth Fund Project (Grant No. 2025ZNSFSC0835). Another project (Grant No. 52305209) is also acknowledged.

CONFLICT OF INTEREST STATEMENT

The authors declare no conflicts of interest.

REFERENCES

[1] M. P. Santosdos. Soares *et al.*, "Towards an effective sensing technology to monitor micro-scale interface loosening of bioelectronic implants," *Sci Rep.*, vol. 11, no. 1, pp. 1–17, 2021.

[2] Y. Lin *et al.*, "Self-powered and autonomous vibrational wake-up system based on triboelectric nanogenerators and MEMS switch," *Sensors*, vol. 22, no. 10, pp. 1–11, 2022.

[3] M. Alhawari *et al.*, *Energy Harvesting for Self-Powered Wearable Devices*, 2018.

[4] B. Otis, and J. Rabaey, *Ultra-low power wireless technologies for sensor networks* (New York, London), 2007.

[5] D. Tan *et al.*, "Wearable bistable triboelectric nanogenerator for harvesting torsional vibration energy from human motion," *Nano Energy.*, vol. 109, p. 108315, 2023.

[6] Y. Zhu *et al.*, "High-power biomechanical energy harvesting from all limb movements of humans," *IEEE/ASME Trans. Mechatron.*, pp. 1–11, 2024.

[7] Z. Zhao *et al.*, "Freestanding flag-type triboelectric nanogenerator for harvesting high-altitude wind energy from arbitrary directions," *ACS Nano*, vol. 10, no. 2, pp. 1780–1787, 2016.

[8] H. Tyagi *et al.*, *Introduction to Solar Energy: Systems, Challenges, and Opportunities*, 2020.

[9] M. L. Seol *et al.*, "Ferrofluid-based triboelectric-electromagnetic hybrid generator for sensitive and sustainable vibration energy harvesting," *Nano Energy*, vol. 31, pp. 233–238, 2017.

[10] H. Zou *et al.*, "Mechanical modulation wave energy harvesting for self-powered marine environment monitoring," *Ocean Eng.*, vol. 314, p. 119683, 2024.

[11] H. Zou *et al.*, "Self-powered wireless gesture control system with liquid metal sensors," *Cell Rep Physical Sci.*, vol. 6, no. 1, p. 102364, 2025.

[12] S. P. Beeby *et al.*, "A micro electromagnetic generator for vibration energy harvesting," *J. Micromech. Microeng.*, vol. 17, no. 7, pp. 1257–1265, 2007.

[13] C. R. Saha *et al.*, "Electromagnetic generator for harvesting energy from human motion," *Sens. Actuators, A*, vol. 147, no. 1, pp. 248–253, 2008.

[14] Y. Xie *et al.*, "High-efficiency ballistic electrostatic generator using microdroplets," *Nat Commun*, vol. 5, no. 4, pp. 1–5, 2014.

[15] Y. Suzuki, "Recent progress in MEMS electret generator for energy harvesting," *IEEJ Trans. Electr. Electron. Eng.*, vol. 6, no. 2, pp. 101–111, 2011.

[16] P. Basset *et al.*, "A batch-fabricated and electret-free silicon electrostatic vibration energy harvester," *J. Micromech. Microeng.*, vol. 19, no. 11, p. 115025, 2009.
[17] L. Qin *et al.*, "A hybrid triboelectric-piezoelectric smart squirrel cage with self-sensing and self-powering capabilities" *Nano Energy*, vol. 124, p. 109506, 2024.
[18] W. Chen *et al.*, "Energy harvesting and vibration reduction by sandwiching piezoelectric elements into elastic damping components with parallel-grooved structures," *Compos. Struct.*, vol. 241, p.112105, 2020.
[19] L. B. Huang *et al.*, "Magnetic-assisted noncontact triboelectric nanogenerator converting mechanical energy into electricity and light emissions" *Adv. Mater.*, vol. 28, no. 14, pp. 2744–2751, 2016.
[20] W. Xu, L. B. Huang, and J. Hao, "Fully self-healing and shape-tailorable triboelectric nanogenerators based on healable polymer and magnetic-assisted electrode," *Nano Energy*, vol. 40, pp. 399–407, 2017.
[21] Y. Su *et al.*, "Hybrid triboelectric nanogenerator for harvesting water wave energy and as a self-powered distress signal emitter," *Nano Energy*, vol. 9, pp. 186–195, 2014.
[22] F. R. Fan, Z. Q. Tian, and Z. Lin. Wang, "Flexible triboelectric generator," *Nano Energy*, vol. 1, no. 2, pp. 328–334, 2012.
[23] H. Zhao and H. Ouyang, "Theoretical investigation and experiment of a disc-shaped triboelectric energy harvester with a magnetic bistable mechanism," *Smart Mater. Struct.*, vol. 30, no. 9, 2021.
[24] S. Gao *et al.*, "Triboelectric based high-precision self-powering cage skidding sensor and application on main bearing of jet engine" *Nano Energy*, vol. 99, p. 107387, 2022.
[25] R. Li *et al.*, "Smart wearable sensors based on triboelectric nanogenerator for personal healthcare monitoring," *Micromachines (Basel)*, vol. 12, no. 4, p. 352, 2021.
[26] Y. Cui *et al.*, "Bio-inspired structures for energy harvesting self-powered sensing and smart monitoring," *Mech. Syst. Sig. Process.*, vol. 228, p. 112459, 2025.
[27] S. Wang *et al.*, "An intelligent planetary gearbox based on ultra-compact triboelectric-electromagnetic hybrid generator," *Nano Energy*, vol. 126, p. 109655, 2024.
[28] J. Yang *et al.*, "Broadband vibrational energy harvesting based on a triboelectric nanogenerator," *Adv. Energy Mater.*, vol. 4, no. 6, pp. 1–9, 2014.
[29] D. Tan *et al.*, "Design and theoretical investigation of a torsional bistable triboelectric nanogenerator," *Int. J. Mech. Sci.*, vol. 236, p. 107760, 2022.
[30] A. Ibrahim, A. Ramini, and S. Towfighian, "Experimental and theoretical investigation of an impact vibration harvester with triboelectric transduction," *J. Sound Vib.*, vol. 416, pp. 111–124, 2018.
[31] C. Zhao *et al.*, "Design, modeling and experimental validation of a low-frequency cantilever triboelectric energy harvester," *Energy*, vol. 214, p. 118885, 2021.
[32] S. Chen *et al.*, "Self-powered cleaning of air pollution by wind driven triboelectric nanogenerator," *Nano Energy*, vol. 14, pp. 217–225, 2014.
[33] Q. Shi *et al.*, "Self-powered triboelectric nanogenerator buoy ball for applications ranging from environment monitoring to water wave energy farm," *Nano Energy*, vol. 40, pp. 203–213, 2017.
[34] X. Chen *et al.*, "A chaotic pendulum triboelectric-electromagnetic hybridized nanogenerator for wave energy scavenging and self-powered wireless sensing system," *Nano Energy*, vol. 69, p. 104440, 2020.
[35] K. Lee *et al.*, "A spherical hybrid triboelectric nanogenerator for enhanced waterwave energy harvesting," *Micromachines (Basel)*, vol. 9, no. 11, pp. 1–11, 2018.
[36] Q. Y. Zhu *et al.*, "Hybrid triboelectric-piezoelectric nanogenerator assisted intelligent condition monitoring for aeroengine pipeline system," *Chem. Eng. J.*, vol. 519, p. 165121, 2025.
[37] L. C. Qin *et al.*, "A hybrid triboelectric-piezoelectric smart squirrel cage with self-sensing and self-powering capabilities," *Nano Energy*, vol. 124, p. 109506, 2024.
[38] J. V. Vidal *et al.*, "Hybrid triboelectric-electromagnetic nanogenerators for mechanical energy harvesting: A review," *Nano-Micro Lett.*, vol. 13, no. 12, pp. 163–220, 2021.
[39] H. Wang *et al.*, "A fully-packaged ship-shaped hybrid nanogenerator for blue energy harvesting toward seawater self-desalination and self-powered positioning," *Nano Energy*, vol. 57, pp. 616–624, 2019.
[40] C. Zhang and Z. L. Wang, *Triboelectric Nanogenerators*, 2018.
[41] T. N. Phan *et al.*, "Design optimization and comparison of cylindrical electromagnetic vibration energy harvesters," *Sensors*, vol. 21, no. 23, p. 7985, 2021.
[42] N. Faedo *et al.*, "On the principle of impedance-matching for underactuated wave energy harvesting systems," *Appl. Ocean Res.*, vol. 118, p. 102958, 2022.
[43] H. Shao *et al.*, "Triboelectric–electromagnetic hybrid generator for harvesting blue energy," *Nano-Micro Lett.*, vol. 10, pp. 198–206, 2018.
[44] T. Quan, *et al.*, "Hybridized electromagnetic-triboelectric nanogenerator for a self-powered electronic watch," *ACS Nano*., vol. 9, pp.12301–12310, 2015.
[45] M. Salauddin and J. Y. Park, "A handy motion driven hybrid energy harvester: Dual Halbach array based electromagnetic and triboelectric generators," *J. Phys. Conf. Ser.*, vol. 773, pp. 3–7, 2016.